IEEE Photonics Journal
An IEEE Photonics Society Publication

Polarization Splitter Based on Soft Glass Nematic Liquid Crystal Photonic Crystal Fiber

Volume 1, Number 6, December 2009

M. F. O. Hameed
S. S. A. Obayya, Senior Member, IEEE

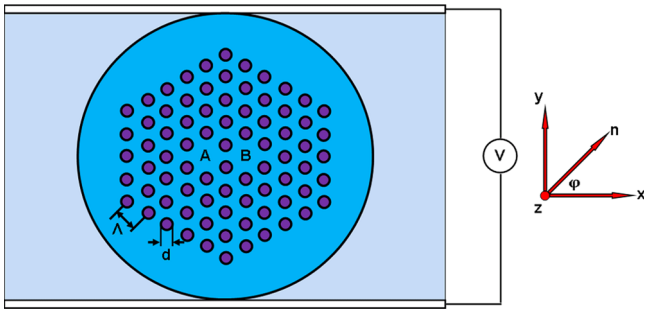

DOI: 10.1109/JPHOT.2009.2037977
1943-0655/$26.00 ©2009 IEEE

Polarization Splitter Based on Soft Glass Nematic Liquid Crystal Photonic Crystal Fiber

M. F. O. Hameed and S. S. A. Obayya, *Senior Member, IEEE*

Faculty of Advanced Technology, University of Glamorgan, Pontypridd, CF37 1DL, U.K.

DOI: 10.1109/JPHOT.2009.2037977
1943-0655/$26.00 ©2009 IEEE

Manuscript received October 22, 2009; revised November 25, 2009. First published Online December 4, 2009. Current version published December 18, 2009. Corresponding author: S. S. A. Obayya (e-mail: sobayya@glam.ac.uk).

Abstract: A novel design of a polarization splitter based on index-guiding soft glass nematic liquid crystal (NLC) photonic crystal fiber is proposed and analyzed. The simulation results are obtained using the full-vectorial finite-difference modal solution along with the full-vectorial finite-difference beam propagation method. The numerical results reveal that the suggested splitter of length 8.227 mm can provide low crosstalk of better than -20 dB with great bandwidths of 30 nm and 75 nm for the quasi TE and TM modes, respectively. In addition, the reported splitter has a tolerance of $\pm 3\%$ in its length, which makes the design less sensitive to the perturbation introduced during the fabrication process.

Index Terms: Photonic crystal fibers, nematic liquid crystal, soft glass, finite-difference method, beam propagation method, couplers and polarization splitters.

1. Introduction

The fiber coupler is one of the most important components in the optical communication systems. It has been shown by Mangan *et al.* [1] that it is possible to use the photonic crystal fiber (PCF) as an optical fiber coupler, which has some advantages compared with conventional optical fiber couplers. PCF couplers can be easily realized by simply introducing two adjacent defects in the PCF. In addition, they have relatively short coupling length and better flexibility design. For these reasons, several studies have been reported for double-core PCF couplers [1]–[6]. Saitoh *et al.* [2] evaluated the coupling characteristics of two different dual core PCF couplers, showing that it is possible to realize significantly shorter multiplexer–demultiplexer PCFs, compared with conventional optical fiber coupler. In addition, a novel design of PCF splitter based on double core PCF with polarization-independent propagation characteristics has been reported in [3]. Moreover, Florous *et al.* [4] proposed a polarization-independent splitter based on highly birefringent dual core PCF, which allows wavelength multiplexing at 1.3 μm and 1.55 μm. Furthermore, a polarization-independent splitter based on index guiding all-silica-based PCF has been suggested in [5].

In order to study the coupling between the TE and TM modes and calculate accurately the modal solution of the input waveguide, the use of full vectorial numerical approaches is mandatory. Over the past few years, various accurate modeling methods have been developed for modal analysis of PCFs, such as the finite-element method (FEM) [7], finite-difference method (FDM) [8], and multipole method [9]. The FEM can provide high accuracy by means of flexible triangular and curvilinear meshes to represent the waveguide cross section. However, this accuracy entails an

algorithm that is complex to implement. On the contrary, the mode solvers based on the FDM and multipole method are very attractive because of their simple implementations. To analyze the propagation through the splitter waveguide section, a more suitable approach such as beam propagation method (BPM) is required. Due to its numerical efficiency and versatility, some full-vectorial BPM algorithms have been formulated based on the FEM [10], [11]. Moreover, many full-vectorial BPM approaches based on the popular FDM have been reported [12], [13].

In this paper, a novel design of polarization splitter based on soft glass PCF infiltrated with a nematic liquid crystal (NLC-PCF) coupler is introduced and investigated through full-vectorial FDM (FVFDM) [8] and full-vectorial finite-difference BPM (FVFD-BPM) [12]. The suggested design depends on using soft glass and nematic liquid crystal (NLC) of types SF57 (lead silica) and E7, respectively. The refractive index of the SF57 material is greater than the ordinary n_o and extraordinary n_e refractive indices of the E7 material which guarantees the index guiding of the light through the NLC-PCF polarization splitter. In addition, the infiltration of the NLC increases the birefringence between the two fundamental polarized modes in the proposed coupler. Therefore, the NLC-PCF coupler has stronger polarization dependence than that of the conventional silica PCF coupler. Also, the soft glass provides optical properties that cannot be obtained by silica, such as high refractive index, high rare-earth solubility, and mid-infrared transmission. The reported splitter has bandwidths (BWs) as great as 30 nm and 75 nm for the quasi TE and TM modes, respectively, with low crosstalk of -20 dB.

The paper is organized as follows. Following this introduction, a brief mathematical analysis is given in Section 2. The design of the NLC-PCF polarization splitter and the simulation results are presented in detail in Section 3. Finally, conclusions are drawn.

2. Mathematical Analysis

The modal solution of the NLC-PCF coupler is performed by the FVFDM [8]. Starting from Maxwell's equations, the vector wave equation for the magnetic field vector can be derived as

$$\nabla \times (\varepsilon^{-1} \nabla \times \mathrm{H}) - \omega^2 \mu_0 \mathrm{H} = 0 \tag{1}$$

where ω is the angular frequency, μ_0 is the permeability of free space, and ε is the permittivity tensor of the waveguide material, which is given by [8], [14]

$$\varepsilon = \varepsilon_0 \varepsilon_r = \varepsilon_0 \begin{pmatrix} \varepsilon_{xx} & \varepsilon_{xy} & 0 \\ \varepsilon_{yx} & \varepsilon_{yy} & 0 \\ 0 & 0 & \varepsilon_{zz} \end{pmatrix} \tag{2}$$

where ε_0 is the permittivity of free space, and ε_r is the relative permittivity tensor of the waveguide material. Using the vector wave equation and the divergence relation $\nabla.\mathrm{H} = 0$, one can obtain, after some algebraic manipulation, the following full-vector eigenvalue equation [8]:

$$\begin{bmatrix} A_{xx} & A_{xy} \\ A_{yx} & A_{yy} \end{bmatrix} \begin{bmatrix} H_x \\ H_y \end{bmatrix} = \beta^2 \begin{bmatrix} H_x \\ H_y \end{bmatrix} \tag{3}$$

where β is the propagation constant, A_{xx}, A_{xy}, A_{yx} and A_{yy} are the differential operators which can be found in detail in [8]. Equation (3) is a full-vector eigenvalue equation, which describes the modes of propagation for an anisotropic optical waveguides. The two transverse field components H_x and H_y are the eigenvectors, and the corresponding eigenvalue is β^2. The differential operators can be approximated by using the FDMs [8] and the robust perfectly matched layer (PML) boundary condition [15] is employed at the edges of the computational window in order to account for the leakage property of the modes. It should be noted that the full-vector eigenvalue equation is solved numerically for a set of modes, and the dominant mode is defined as the mode with the highest real effective index value. Since $\nabla.\mathrm{H} = 0$ and interface boundary conditions are automatically satisfied in the formulation, then there is no chance for spurious (nonphysical) modes to appear in the spectrum of the solution.

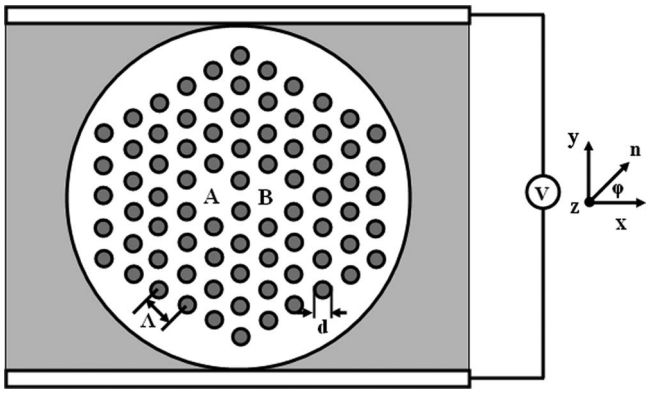

Fig. 1. Cross section of the NLC-PCF coupler sandwiched between two electrodes and surrounded by silicone oil. The director of the NLC with a rotation angle φ is shown at the right.

The beam propagation analysis of the reported splitter is evaluated by the FVFD-BPM [12], which can be described as follows. By letting $H_t = \widehat{H}_t e^{-jkn_o z}$ and assuming the slowly varying approximation [12], one can obtain, after some algebraic manipulation, the following two equations:

$$[1 + j\Delta z \alpha B_{xx}]\widehat{H}_x^{L+1} = [1 - j\Delta z(1-\alpha)B_{xx}]\widehat{H}_x^{L} - j\Delta z B_{xy}\widehat{H}_y^{L} \quad (4)$$

$$[1 + j\Delta z \alpha B_{yy}]\widehat{H}_y^{L+1} = [1 - j\Delta z(1-\alpha)B_{yy}]\widehat{H}_y^{L} - j\Delta z B_{yx}\widehat{H}_x^{L} \quad (5)$$

where n_o is the reference index which is used to satisfy the slowly varying envelope approximation, α is introduced to control the scheme used to solve the finite-difference equations, B_{xx}, B_{xy}, B_{yx}, and B_{yy} are the new differential operators which can be obtained from [8], [12]. The new differential operators are also approximated using the FDM [8]. Equations (4) and (5) for the transverse magnetic fields are solved by an iterative procedure to get the required magnetic fields. The magnetic fields, $\widehat{H}_x^{L+1}$ and $\widehat{H}_y^{L+1}$ at a distance $L+1$ in the *z*-direction can be obtained from the previous magnetic fields, $\widehat{H}_x^{L}$ and $\widehat{H}_y^{L}$, respectively at a distance L in the *z*-direction.

3. Design and Numerical Results

The cross section of the proposed NLC-PCF coupler is shown in Fig. 1. The cladding holes have been infiltrated with a NLC of type E7 and arranged in a soft glass background. The infiltrated holes of diameter d are arranged in a triangular lattice with hole pitch Λ. The separation between the centers of the two cores, A and B, shown in Fig. 1 is equal to $\sqrt{3}\Lambda$. The NLCs considered in the proposed structure are anisotropic materials consisting of rod-like molecules which are characterized by ordinary index n_o and extraordinary index n_e. Moreover, the local orientation of the NLCs as shown in Fig. 1 is described by its director, which is a unit vector n along the direction of the average orientation of the molecules.

Having applied a static electric field, the director's orientation can be controlled, since the liquid crystal molecules tend to align their axis according to the applied field. Therefore, the fiber is placed between two pairs of electrodes [16] allowing for the arbitrary control of the alignment of the NLC director via an external voltage, as schematically shown in Fig. 1. Additionally, two silica rods with appropriate diameters are used to control the spacing between the electrodes and the fiber is surrounded by silicone oil, which has higher dielectric strength than air. Therefore, the external electric field as reported by Haakestad *et al.* [16] will be uniform across the fiber cross section which results in good alignment of the director of the NLC with constant rotation angle φ. Moreover, the nonuniform electric field region will be only at the edges far away from the cores where the light will be propagating. As a result, the proposed coupler overall performance will avoid the nonuniform field distribution. Other layouts, such as those described

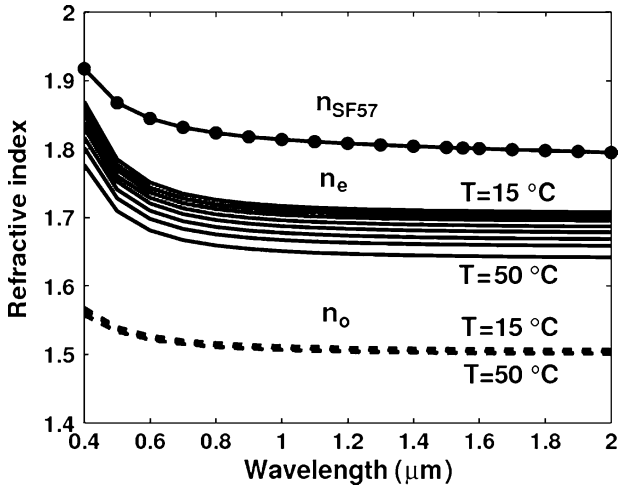

Fig. 2. Variation of n_o and n_e of the E7 material with the wavelength at different temperatures T from 15 °C to 50 °C with a step of 5 °C [30]. The solid line with closed circles represents the variation of the refractive index of the SF57 material with the wavelength [22].

in [17] and [18], can also be used to ensure better field distribution uniformity over the fiber cross section.

The practical techniques that have been utilized in the manufacturing of the nonsilica PCF are capillary stacking [19], drilling [20], build-in casting [21], and extrusion [22]–[24]. However, extrusion mechanism offers a controlled and reproducible approach for fabricating complex structured PCFs with a considerable surface quality. Furthermore, extrusion can be used to produce structures that could not be created with the capillary stacking approaches. Therefore, in the literature, most of the fabricated nonsilica PCFs are based on extrusion. Recently, the extrusion approach has been extended to construct the soft glasses such as lead silicate (SF57 glass) [22]–[24] and tellurite [25]. The soft glass of type SF57 has low processing temperature of $\sim$520 °C [26], while the softening temperature for silica glass is 1500–1600 °C. Therefore, it is possible to extrude the PCF preform directly from the bulk glass. Also, lead silicate glasses [22] offer the highest thermal and crystallization stability making them particularly attractive for PCF fabrication.

The filling of PCFs with liquid or liquid-crystalline materials has already been demonstrated in the literature [16], [18], [27]–[29]. Arc-fusion techniques have been successfully implemented for the infiltration of central defect cores [28], while extensive control in the infiltration process of either core or cladding capillaries can be achieved by using UV curable polymers [29]. In [16], all the cladding holes of the PCF are filled with NLC using capillary forces and an electrically tunable photonic bandgap guidance is reported. In addition, tunable light switch using PCF whose central defect and cladding holes are filled with NLC is studied by Fang *et al.* [18].

The ordinary n_o and extraordinary n_e refractive indices of the E7 material were measured previously by J. Li *et al.* [30] at different visible wavelengths in the temperature range from 15 °C to 50 °C with a step of 5 °C. Then, the Cauchy model was adopted to fit the measured n_o and n_e, which can be described as follows [30]:

$$n_e = A_e + (B_e/\lambda^2) + (C_e/\lambda^4) \tag{6}$$

$$n_o = A_o + (B_o/\lambda^2) + (C_o/\lambda^4) \tag{7}$$

where A_e, B_e, C_e, A_o, B_o and C_o are the coefficients of the Cauchy model. The Cauchy coefficients at T = 25 °C are $A_e = 1.6933$, $B_e = 0.0078\ \mu m^2$, $C_e = 0.0028\ \mu m^4$, $A_o = 1.4994$, $B_o = 0.0070\ \mu m^2$, and $C_o = 0.0004\ \mu m^4$. Fig. 2 shows the wavelength dependence n_o and n_e of the E7 material at different temperatures T from 15 °C to 50 °C with a step of 5 °C. It is evident from this figure that n_e is

greater than n_o at the measured temperature values within the reported wavelength range. In the proposed design, the relative permittivity tensor ε_r of the E7 material is taken as [14]

$$\varepsilon_r = \begin{pmatrix} n_o^2 \sin^2\varphi + n_e^2 \cos^2\varphi & (n_e^2 - n_o^2)\cos\varphi\sin\varphi & 0 \\ (n_e^2 - n_o^2)\cos\varphi\sin\varphi & n_o^2\cos^2\varphi + n_e^2\sin^2\varphi & 0 \\ 0 & 0 & n_o^2 \end{pmatrix} \tag{8}$$

where φ is the rotation angle of the director of the NLC, as shown in Fig. 1. The proposed in-plane alignment of the NLC can be exhibited under the influence of an appropriate homeotropic anchoring conditions [14], [31]. Haakestad *et al.* [16] demonstrated experimentally that in the strong field limit, the NLC of type E7 is aligned in plane in *y*-direction in capillaries of diameter 5 μm. Moreover, Alkeskjold and Bjarklev [32] presented in-plane alignment with three different rotation angles, 0°, 45°, and 90° in solid core PCF with hole diameter of 3 μm infiltrated with NLC of type E7 using two sets of electrodes.

The background material of the reported NLC-PCF coupler is a soft glass of type SF57 (lead silica). Fig. 2 shows the wavelength-dependent refractive index of the SF57 material. As revealed from this figure, the refractive index of the SF57 material is larger than n_o and n_e of the E7 material. Therefore, the average refractive index of the soft glass core is greater than that of the infiltrated NLC cladding region. Consequently, the propagation through the suggested design has been taken place by the modified total internal reflection The Sellmeier equation of the soft glass of type SF57 [22] is given by

$$n_{SF57}^2 = A_o + A_1\lambda^2 + \frac{A_2}{\lambda^2} + \frac{A_3}{\lambda^4} + \frac{A_4}{\lambda^6} + \frac{A_5}{\lambda^8} \tag{9}$$

where n_{SF57} is the refractive index of the SF57 material, $A_o = 3.24748$, $A_1 = -0.00954782\ \mu m^{-2}$, $A_2 = 0.0493626\ \mu m^2$, $A_3 = 0.00294294\ \mu m^4$, $A_4 = -1.48144 \times 10^{-4}\ \mu m^6$, and $A_5 = 2.78427 \times 10^{-5}\ \mu m^8$ [22].

In the proposed design, the cladding holes have the same diameter d and are arranged with a hole pitch $\Lambda = 2.0\ \mu$m. In addition, n_o, n_e, n_{SF57} are taken as 1.5024, 1.6970, and 1.802, respectively, at the operating wavelength $\lambda = 1.55\ \mu$m. Moreover, the rotation angle of the director of the NLC and the temperature are taken as 90° and 25 °C, respectively. The effective indices of the even mode n_{eff_e} and odd mode n_{eff_o} of the NLC-PCF coupler are evaluated by the FVFDM [8] with perfect matched layer boundary conditions. The coupling length, defined as the minimum longitudinal distance at which maximum power is transferred from one core to another, is one of the important characteristics of the directional couplers. The coupling length L_C can be obtained using the operating wavelength λ, n_{eff_e} and n_{eff_o} as follows:

$$L_C = \frac{\lambda}{2(n_{eff\_e} - n_{eff\_o})}. \tag{10}$$

Fig. 3 shows the variation of the coupling lengths of the NLC-PCF coupler for the quasi TE and TM modes with the d/Λ ratio at the operating wavelength of 1.55 μm while the hole pitch, is fixed to 2 μm. It is observed from this figure that the coupling lengths for the two polarized modes increase with increasing the d/Λ ratio at constant hole pitch Λ. As the d/Λ ratio increases at constant Λ, the soft glass bridge between the two cores of the NLC-PCF coupler decreases. Therefore, the distance taken by the modes to transfer between the two cores and, hence, the coupling lengths of the two polarized modes increases. As the d/Λ ratio increases from 0.6 to 0.85, the coupling lengths of the quasi TE and TM modes increase from 429 μm and 241 μm to 1914 μm and 454 μm, respectively. It is also evident from Fig. 3 that the coupling length of the quasi TE mode at $\varphi = 90°$ is longer than that of the quasi TM mode. This can be explained by analyzing the dominant field components of the quasi TE and TM modes and the direction of the director of the NLC. The dominant field components of the quasi TE and TM modes are E_x and E_y, respectively. At $\varphi = 90°$, the director of the NLC is parallel to E_y while it is perpendicular to E_x, and the relative permittivity tensor ε_r of the E7 material has the diagonal form $[n_o^2, n_e^2, n_o^2]$. In this case, ε_{yy} is greater than ε_{xx}, and therefore, the

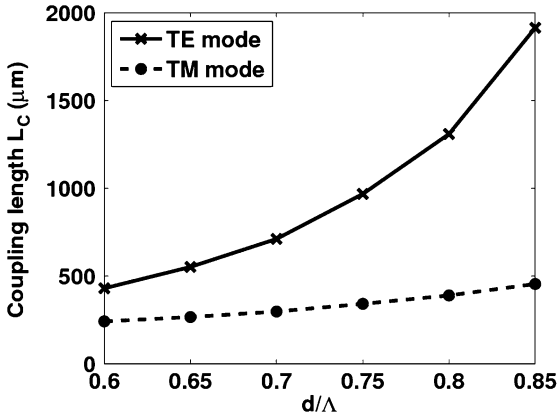

Fig. 3. Variation of the coupling lengths of the two polarized modes with the d/Λ ratio while the hole pitch, rotation angle of the director of the NLC, temperature, and wavelength are fixed to 2 μm, 90°, 25 °C, and 1.55 μm, respectively.

index contrast seen by the quasi TE mode is greater than that seen by the quasi TM mode. Consequently, the quasi TE modes are more confined in the core regions than the quasi TM modes. As a result, the quasi TE modes take longer distance than the quasi TM modes to transfer from one core to another and hence the coupling lengths of the quasi TE modes are longer than those of the quasi TM modes.

It is also revealed from Fig. 3 that the NLC-PCF coupler has strong polarization dependence. This is due to the infiltration of the NLC which increases the birefringence between the two fundamental polarized modes in the proposed coupler. Therefore, the NLC-PCF coupler can be easily designed as a polarization splitter and its polarization dependence is stronger than those splitters presented in [6], [33], and [34]. However, the conventional silica PCF coupler [2] has low birefringence and the high birefringence can be realized by adjusting the size of the air holes around the two core regions [6], [33], [34], which enlarges the difference between the coupling lengths for the two polarized modes. In [33], the two identical cores are formed by combination of large and small air holes which makes the two cores birefringent. Zhang and Yang [34] reported a polarization splitter based on two nonidentical cores with also a combination of large and small air holes. However, in [6], two elliptical cores are used to improve the polarization dependence of the conventional silica PCF coupler.

The fiber coupler can separate the two polarized states, i.e., quasi TE and TM modes, at a given wavelength if the coupling lengths L_{CTE} and L_{CTM} of the quasi TE and TM modes, respectively, satisfy the coupling ratio [5]

$$\gamma = L_{CTE} : L_{CTM} = i : j \tag{11}$$

where i and j are two integers of different parities. In this case, the length of the coupler is equal to $L_f = L_{CTM} \times i/j$. Therefore, to achieve the shortest splitter, the optimal value of γ should be 2. Fig. 4 shows the coupling length ratio between the coupling lengths of the quasi TE and TM modes as a function of the d/Λ ratio at two different hole pitch values: 3.7 μm and 3.9 μm. In this study, the operating wavelength, rotation angle of the director of the NLC and temperature are taken as 1.55 μm, 90°, and 25 °C, respectively. It is found that the coupling length ratio γ increases with increasing the d/Λ ratio at a given hole pitch while the crosstalk decreases as revealed from Figs. 4 and 5. The crosstalk is a measure of the unwanted power, remaining at the end of the NLC-PCF coupler. Fig. 5 shows the variation of the crosstalk for the quasi TE and TM modes with the d/Λ ratio at the operating wavelength $\lambda = 1.55$ μm at two different hole pitch values: 3.7 μm and 3.9 μm. As shown from this figure, the crosstalk of the quasi TE is lower than that of the quasi TM mode due to the better confinement of the quasi TE modes through the core regions than the quasi TM mode at

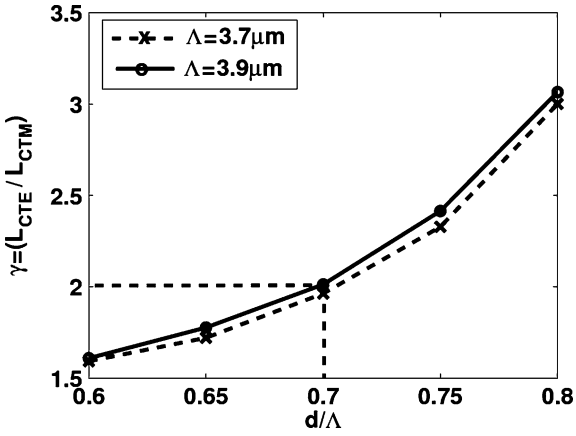

Fig. 4. Variation of the coupling length ratio for the quasi TE and TM modes of the NLC-PCF coupler with the d/Λ ratio at two different hole pitch values Λ, 3.7 μm, and 3.9 μm while the operating wavelength is fixed to $\lambda = 1.55$ μm.

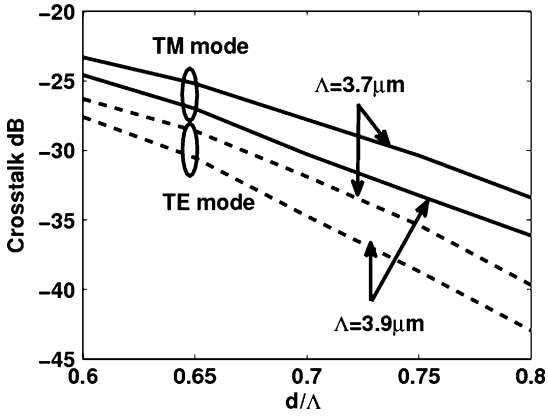

Fig. 5. Variation of the crosstalk for the quasi TE and TM modes of the NLC-PCF coupler with the d/Λ ratio at two different hole pitch values Λ, 3.7 μm, and 3.9 μm while the operating wavelength is fixed to $\lambda = 1.55$ μm.

$\varphi = 90^{\circ}$. As can be seen from Fig. 4, the coupling length ratio equals 2.013 at $d/\Lambda = 0.7$ and hole pitch of 3.9 μm. The coupling lengths calculated by the FVFDM are 8252 μm and 4099 μm for the quasi TE and TM modes, respectively at the operating wavelength $\lambda = 1.55$ μm.

In order to confirm the polarization splitter based on the NLC-PCF coupler, the FVFD-BPM is used to study the propagation along its axial direction. Initially, at $z = 0$, the fundamental components H_y and H_x of the quasi TE and TM modes, respectively of soft glass PCF with air holes obtained using the FVFDM [8] at $\lambda = 1.55$ μm are launched into the left core A of the NLC-PCF coupler. These input fields, in turn, start to transfer to the right core of the coupler, and at the corresponding coupling lengths, the fields are completely transferred to the right core. The coupling lengths calculated by the FVFD-BPM are 8253 μm and 4100 μm for the quasi TE and TM modes, respectively, which are in excellent agreement with those obtained by the FVFDM. The ratio between the coupling lengths L_{CTE} to L_{CTM} is slightly larger than 2.0. Therefore, the length of the proposed coupler is $L_f = (8253 + 2 * 4100)/2.0 = 8227$ μm at which the two polarized states are separated well. Fig. 6 shows the power transfer normalized to the input power for the quasi TE and TM modes at the operating wavelength of 1.55 μm in the left core of the NLC-PCF coupler. It is evident from Fig. 6 that the two polarized modes are separated well after a propagation distance equals to $L_f = 8227$ μm. The normalized powers of the quasi TE mode in the left and right cores of

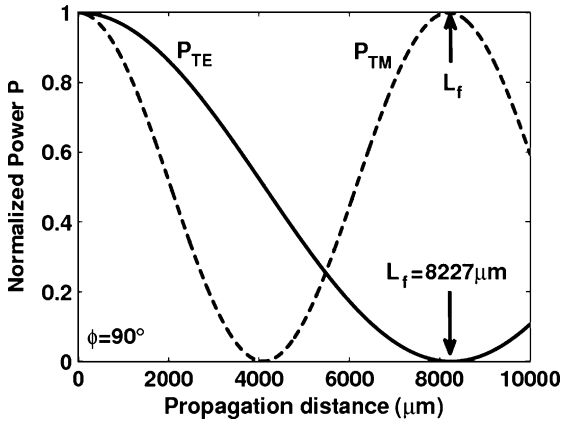

Fig. 6. Evolution of the normalized powers at the left core A for the quasi TE and TM modes at the operating wavelength of 1.55 μm along the propagation direction.

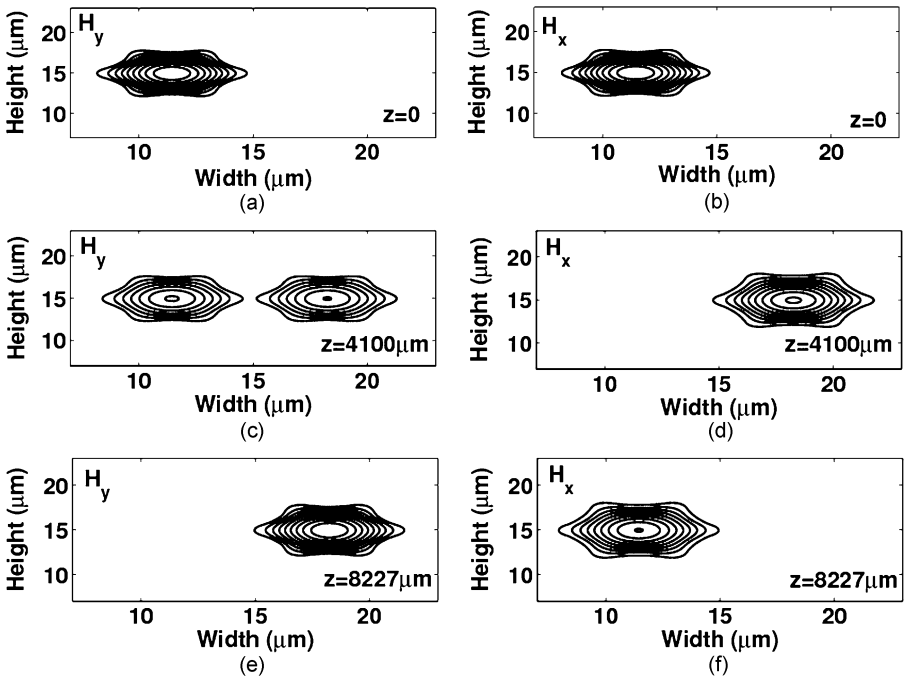

Fig. 7. Field contour patterns for H_y and H_x of the quasi TE and TM modes, respectively, at z, 0, 4100 μm, and 8227 μm at $\lambda = 1.55$ μm.

the coupler are 0.000435 and 0.9995, respectively, at z = 8227 μm. However, the normalized powers of the quasi TM mode in the left and right cores of the coupler are 0.9987 and 0.0013, respectively. Therefore, when launched from one end of the splitter, the signals of the quasi TE mode will exit at the other core B, while the signals of the quasi TM mode will exit at the same core A.

The field distributions of the dominant field component H_y and H_x of the quasi TE and TM modes, respectively at $\lambda = 1.55$ μm are shown in Fig. 7 at different waveguide sections z, 0, 4100 μm, and 8227 μm. It is evident from this figure that, at z = 0, the input fields are launched into the left core, and as the propagation distance increases, the normalized power in the right core increases, and that in the left core decreases. At z = 4100 μm, which is equal to the coupling length of the quasi

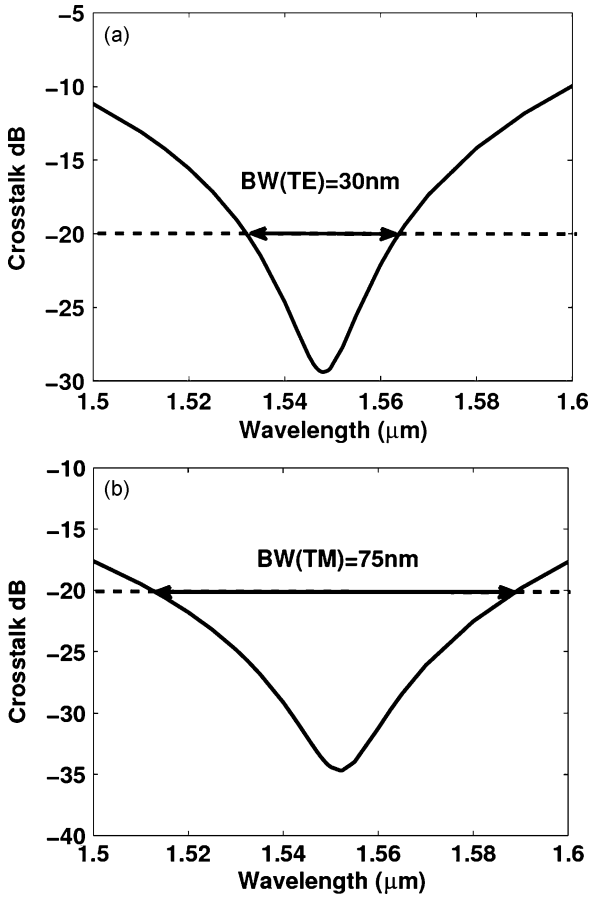

Fig. 8. Wavelength dependence crosstalk of the NLC-PCF coupler around the operating wavelength $\lambda = 1.55$ μm for the (a) quasi TE and (b) quasi TM modes.

TM mode, the normalized power of quasi TM mode is approximately completely transferred to the right core. The normalized powers of the quasi TM mode in the left and right cores of the coupler are 0.00096 and 0.99904, respectively. However, the normalized powers of the quasi TE mode in the left and right cores of the coupler are 0.5051 and 0.4949, respectively, at z = 4100 μm. Finally, the two polarized modes are separated after a propagation distance $L_f = 8227$ μm.

The crosstalk CT around the operating wavelength $\lambda = 1.55$ μm for the quasi TE and TM modes are shown in Fig. 8(a) and (b), respectively. The crosstalk in decibel [3] for the desired quasi TE mode at the right core B is defined such that

$$CT_{TE} = 10\log_{10}(P_{B,uTM}/P_{B,dTE}) \tag{12}$$

where $P_{B,dTE}$ and $P_{B,uTM}$ are the normalized power of the desired quasi TE and undesired quasi TM modes, respectively, at core B. However, the crosstalk [3] of the desired quasi TM mode at the left core A is given by

$$CT_{TM} = 10\log_{10}(P_{A,uTE}/P_{A,dTM}) \tag{13}$$

where $P_{A,uTE}$ and $P_{A,dTM}$ are the normalized power of the undesired quasi TE and desired quasi TM modes, respectively, at core A. It is revealed form Fig. 8 that the proposed splitter has large BWs of 30 nm and 75 nm for the quasi TE and TM modes, respectively, at which the crosstalks are better than -20 dB. In addition, the BWs are 15 nm and 42 nm for the quasi TE and TM modes, respectively, for the crosstalks that are lower than -25 dB. Therefore, the proposed polarization

splitter is less sensitive to the perturbation introduced during the fabrication process due to the low-level crosstalks with wide wavelength ranges. The BWs of the NLCPCF splitter are much larger than those reported in [3] and [4]. The BW of the quasi TE mode in [3] is 2.7 nm around $\lambda = 1.55$ μm, while the BW in [4] is 2.0 nm. In addition, the proposed splitter is shorter than those reported in [3] and [4] of lengths 15.4 mm and 9.08 mm, respectively. Moreover, the NLC-PCF splitter has wide wavelength range larger than the reported splitter by Chen *et al.* [5] of BW 25.4 nm around $\lambda = 1.55$ μm for the quasi TE mode. Furthermore, the splitter in [5] has longer length of 10.69 mm than that of the NLC-PCF splitter.

It is also shown from Fig. 8, that the BW of the quasi TE mode is less than that of the quasi TM mode. At $\varphi = 90°$, the quasi TE mode is more confined through the core region than the quasi TM mode. Therefore, the quasi TM mode is more affected by the wavelength variation around $\lambda = 1.55$ μm than the quasi TE mode. As a result, the undesired normalized power of the quasi TM mode at core B at the device length of 8227 μm increases with the wavelength variation around $\lambda = 1.55$ μm more than the undesired normalized power of the quasi TE mode at core A. Therefore, the BW of the quasi TE mode at core B is less than that of the quasi TM mode at core A.

The tolerances of the fiber length, rotation angle φ of the director of the NLC and temperature are also investigated. It is worth noting that the tolerance of a specific parameter is calculated while the other parameters of the proposed design are kept constant. It is found that the fiber length and rotation angle φ allow a tolerance of $\pm 3\%$ and $\pm 5°$, respectively, at which the crosstalks are still better than -20 dB.

As shown in Fig. 2, the ordinary n_o and extraordinary n_e refractive indices of the E7 material are influenced by the temperature variation which affects the coupling characteristics of the NLC-PCF coupler. It can be observed from Fig. 2 that n_e of the E7 material is more dependent on the temperature than n_o. As the temperature T increases from 15 °C to 50 °C, n_e of the E7 material decreases from 1.7096 to 1.6438 at the operating wavelength $\lambda = 1.55$ μm. However, n_o of the E7 material decreases slightly from 1.5034 to 1.5017 when the temperature changes from 15 °C to 35 °C, while n_o increases from 1.5017 to 1.5089 when T increases from 35 °C to 50 °C. Therefore, the tolerance of the temperature is the next parameter to be studied while the other parameters of the reported design are not modified. It is found that the crosstalk of the quasi TM mode is better than -30 dB over a temperature range from 15 °C to 50 °C. However, the crosstalk of the quasi TE mode has a tolerance of ± 5 °C at which the crosstalk is better than -14 dB. This can be explained as follows. At $\varphi = 90°$, the relative permittivity tensor ε_r of the E7 material has the diagonal form $[n_o^2, n_e^2, n_o^2]$. Therefore, as the temperature increases, ε_{yy} decreases while ε_{xx} is nearly invariant. As a result, the index contrast seen by the quasi TM mode increases by increasing the temperature which increases the confinement of the quasi TM mode through the core regions. Thus, the coupling length of the quasi TM mode increases with increasing the temperature. However, the index contrast seen by the quasi TE mode and, hence, its coupling length is nearly constant with the temperature variation. Therefore, the undesired normalized power of the quasi TM mode at core B at the device length of 8227 μm increases, which increases the crosstalk of the quasi TE mode. On the other hand, the undesired power of the quasi TE modes at core A is approximately invariant, which has little effect on the crosstalk of the quasi TM mode.

4. Conclusion

A novel type of polarization splitter based on NLC-PCF coupler has been presented and analyzed. The results are evaluated using the FVFDM and confirmed by the FVFD-BPM. It is evident from the simulation results that the NLC-PCF splitter has advantages in terms of its short coupling length as well as the low crosstalk over large optical BWs. The suggested splitter has a length of 8.227 mm with a crosstalk better than -20 dB with BWs of 30 nm and 75 nm for the quasi TE and TM modes, respectively. In addition, the splitter has a tolerance of $\pm 3\%$ in its length, which makes the design more robust to the perturbation introduced during the fabrication. Moreover, the rotation angle of the director of the NLC has a tolerance of $\pm 5°$, at which the crosstalks are better than -20 dB. Furthermore, the crosstalk of the quasi TM mode is better than -30 dB over a temperature range

from 15 °C to 50 °C. However, the crosstalk of the TE mode has a tolerance of ±5 °C, at which the crosstalk is better than −14 dB.

References

[1] B. J. Mangan, J. C. Knight, T. A. Birks, P. S. J. Russell, and A. H. Greenaway, "Experimental study of dual core photonic crystal fiber," *Electron. Lett.*, vol. 36, no. 16, pp. 1358–1359, Aug. 2000.

[2] K. Saitoh, Y. Sato, and M. Koshiba, "Coupling characteristics of dual-core photonic crystal fiber couplers," *Opt. Express*, vol. 11, no. 24, pp. 3188–3195, Dec. 2003.

[3] N. Florous, K. Saitoh, and M. Koshiba, "A novel approach for designing photonic crystal fiber splitters with polarization-independent propagation characteristics," *Opt. Express*, vol. 13, no. 19, pp. 7365–7373, Sep. 2005.

[4] N. J. Florous, K. Saitoh, and M. Koshiba, "Synthesis of polarization-independent splitters based on highly birefringent dual-core photonic crystal fiber platforms," *IEEE Photon. Technol. Lett.*, vol. 18, no. 11, pp. 1231–1233, Jun. 2006.

[5] M. Y. Chen and J. Zhou, "Polarization-independent splitter based on all-solid silica-based photonic-crystal fibers," *J. Lightw. Technol.*, vol. 24, no. 12, pp. 5082–5086, Dec. 2006.

[6] L. Zhang and C. Yang, "Polarization-dependent coupling in twin-core photonic crystal fibers," *J. Lightw. Technol.*, vol. 22, no. 5, pp. 1367–1373, May 2004.

[7] S. S. A. Obayya, B. M. A. Rahman, K. T. V. Grattan, and H. A. El-Mikati, "Full vectorial finite-element-based imaginary distance beam propagation solution of complex modes in optical waveguides," *J. Lightw. Technol.*, vol. 20, no. 6, pp. 1054–1060, Jun. 2002.

[8] A. B. Fallahkhair, K. S. Li, and T. E. Murphy, "Vector finite difference modesolver for anisotropic dielectric waveguides," *J. Lightw. Technol.*, vol. 26, no. 11, pp. 1423–1431, Jun. 2008.

[9] S. Campbell, R. C. McPhedran, C. Martijn de Sterke, and L. C. Botten, "Differential multipole method for microstructured optical fibers," *J. Opt. Soc. Amer. B, Opt. Phys.*, vol. 21, no. 11, pp. 1919–1928, Nov. 2004.

[10] S. S. A. Obayya, B. M. A. Rahman, and H. A. El-Mikati, "New full vectorial numerically efficient propagation algorithm based on the finite element method," *J. Lightw. Technol.*, vol. 18, no. 3, pp. 409–415, Mar. 2000.

[11] E. Montanari, S. Selleri, L. Vincetti, and M. Zoboli, "Finite element full vectorial propagation analysis for three dimensional z-varying optical waveguides," *J. Lightw. Technol.*, vol. 16, no. 4, pp. 703–714, Apr. 1998.

[12] W. P. Huang and C. L. Xu, "Simulation of three-dimensional optical waveguides by a full-vector beam propagation method," *IEEE J. Quantum Electron.*, vol. 29, no. 10, pp. 2639–2649, Oct. 1993.

[13] J. Xiao and X. Sun, "A modified full-vectorial finite-difference beam propagation method based on H-fields for optical waveguides with step-index profiles," *Opt. Commun.*, vol. 266, no. 2, pp. 505–511, Oct. 2006.

[14] G. Ren, P. Shum, X. Yu, J. Hu, G. Wang, and Y. Gong, "Polarization dependent guiding in liquid crystal filled photonic crystal fibers," *Opt. Commun.*, vol. 281, no. 6, pp. 1598–1606, Mar. 15, 2008.

[15] W. C. Chew, J. M. Jin, and E. Michielssen, "Complex coordinate stretching as a generalized absorbing boundary condition," *Microw. Opt. Technol. Lett.*, vol. 15, no. 6, pp. 363–369, Aug. 1997.

[16] M. W. Haakestad, T. T. Alkeskjold, M. Nielsen, L. Scolari, J. Riishede, H. E. Engan, and A. Bjarklev, "Electrically tunable photonic bandgap guidance in a liquid-crystal-filled photonic crystal fiber," *IEEE Photon. Technol. Lett.*, vol. 17, no. 4, pp. 819–821, Apr. 2005.

[17] B. R. Acharya, K. W. Baldwin, J. A. Rogers, C. C. Huang, and R. Pindak, "In-fiber nematic liquid crystal optical modulator based on in-plane switching with microsecond response time," *Appl. Phys. Lett.*, vol. 81, no. 27, pp. 5243–5245, Dec. 2002.

[18] D. Fang, Q. L. Yan, and T. W. Shin, "Electrically tunable liquid-crystal photonic crystal fiber," *Appl. Phys. Lett.*, vol. 85, no. 12, pp. 2181–2183, Sep. 2004.

[19] J. C. Knight, T. A. Birks, P. S. J. Russell, and D. M. Atkin, "All-silica single-mode fiber with photonic crystal cladding," *Opt. Lett.*, vol. 21, no. 19, pp. 1547–1549, Oct. 1996.

[20] A. Mori, K. Shikano, K. Enbutsu, K. Oikawa, K. Naganuma, M. Kato, and S. Aozasa, "1.5μm band zero-dispersion shifted tellurite photonic crystal fibre with a nonlinear coefficient of 675 W-1km-1," presented at the 30th Eur. Conf. Optical Commun., Stockholm, Sweden, 2004, Paper Th3.3.6.

[21] X. Feng, A. K. Mairaj, D. W. Hewak, and T. M. Monro, "Towards high-index glass based monomode holey fibre with large-mode-area," *Electron. Lett.*, vol. 40, no. 3, pp. 167–169, Feb. 2004.

[22] J. Y. Y. Leong, "Fabrication and applications of lead-silicate glass holey fibre for 1–1.5 microns: Nonlinearity and dispersion trade offs," Ph.D. dissertation, Faculty Eng., Sci. Math. Optoelectron. Res. Centre, Univ. Southampton, Southampton, U.K., 2007.

[23] P. Petropoulos, T. M. Monro, H. Ebendorff-Heidepriem, K. Frampton, R. C. Moore, and D. J. Richardson, "Highly nonlinear and anomalously dispersive lead silicate glass holey fibres," *Opt. Express*, vol. 11, no. 26, pp. 3568–3573, Dec. 2003.

[24] K. M. Kiang, K. Frampton, T. M. Monro, R. Moore, J. Tucknott, D. W. Hewak, D. J. Richardson, and H. N. Rutt, "Extruded single-mode nonsilica glass holey optical fibres," *Electron. Lett.*, vol. 38, no. 12, pp. 546–547, Jun. 2002.

[25] V. Kumar, A. K. George, J. C. Knight, and P. S. J. Russell, "Tellurite photonic crystal fibre," *Opt. Express*, vol. 11, no. 20, pp. 2641–2645, Oct. 2003.

[26] S. Fujino, H. Ijiri, F. Shimizu, and K. Morinaga, "Measurement of viscosity of multi-component glasses in the wide range for fibre drawing," *J. Jpn. Inst. Met.*, vol. 62, no. 1, pp. 106–110, 1998.

[27] K. Nielsen, D. Noordegraaf, T. Sørensen, A. Bjarklev, and T. P. Hansen, "Selective filling of photonic crystal fibers," *J. Opt. A, Pure Appl. Opt.*, vol. 7, no. 8, pp. L13–L20, Aug. 2005.

[28] L. Xiao, W. Jin, M. S. Demokan, H. L. Ho, Y. L. Hoo, and C. Zhao, "Fabrication of selective injection microstructured optical fibers with a conventional fusion splicer," *Opt. Express*, vol. 13, no. 22, pp. 9014–9022, Oct. 2005.

[29] Y. Huang, Y. Xu, and A. Yariv, "Fabrication of functional microstructured optical fibers through a selective-filling technique," *Appl. Phys. Lett.*, vol. 85, no. 22, pp. 5182–5184, Nov. 2004.
[30] J. Li, W. Shin-Tson, B. Stefano, M. Riccardo, and F. Sandro, "Infrared refractive indices of liquid crystals," *J. Appl. Phys.*, vol. 97, no. 7, pp. 073 501-1–073 501-5, Apr. 2005.
[31] D. C. Zografopoulos, E. E. Kriezis, and T. D. Tsiboukis, "Photonic crystal-liquid crystal fibers for single-polarization or high-birefringence guidance," *Opt. Express*, vol. 14, no. 2, pp. 914–925, Jan. 2006.
[32] T. T. Alkeskjold and A. Bjarklev, "Electrically controlled broadband liquid crystal photonic bandgap fiber polarimeter," *Opt. Lett.*, vol. 32, no. 12, pp. 1707–1709, Jun. 2007.
[33] L. Zhang and C. Yang, "Polarization splitter based on photonic crystal fibers," *Opt. Express*, vol. 11, no. 9, pp. 1015–1020, May 2003.
[34] L. Zhang and C. Yang, "A novel polarization splitter based on the photonic crystal fiber with nonidentical dual cores," *IEEE Photon. Technol. Lett.*, vol. 16, no. 7, pp. 1670–1672, Jul. 2004.